molecular microbiology

Characterisation of the *Toxoplasma gondii* tyrosine transporter and its phosphorylation by the calcium-dependent protein kinase 3

Journal:	*Molecular Microbiology*
Manuscript ID	MMI-2018-17273.R1
Manuscript Type:	Research Article
Date Submitted by the Author:	12-Oct-2018
Complete List of Authors:	Wallbank, Bethan; Francis Crick Institute, Parasitology Dominicus, Caia; The Francis Crick Institute, Signalling in Apicomplexan parasites laboratory Broncel, Malgorzata; The Francis Crick Institute, Signalling in Apicomplexan parasites laboratory Legrave, Nathalie; The Francis Crick Institute, Metabolomics science technology platform MacRae, James; The Francis Crick Institute, Metabolomics science technology platform Staines, Henry; St George's, University of London, CMM-Infectious Diseases; Treeck, Moritz ; The Francis Crick Institute, Signalling in Apicomplexan parasites laboratory
Key Words:	Parasitology, Toxoplasma, Signalling, Amino acid transporter

Characterisation of the *Toxoplasma gondii* tyrosine transporter and its phosphorylation by the calcium-dependent protein kinase 3

Short Title: Characterisation of a tyrosine transporter in *Toxoplasma gondii*

Bethan A. Wallbank[1], Caia S. Dominicus[1], Malgorzata Broncel[1], Nathalie Legrave[2], James I. MacRae[2], Henry M. Staines[3] and Moritz Treeck[1*]

[1] Signalling in Apicomplexan Parasites Laboratory, The Francis Crick Institute, London, United Kingdom

[2] Metabolomics Science Technology Platform, The Francis Crick Institute, London, United Kingdom

[3] St George's, University of London, Institute of Infection and Immunity, London, United Kingdom

* Corresponding author (MT) Moritz.treeck@crick.ac.uk, +44 20 3796 2345

Keywords: *Toxoplasma*, tyrosine, transporter, CDPK3, phosphorylation

The authors confirm that there are no conflicts of interest with the contents of this article.

For Peer Review

Summary

Toxoplasma gondii parasites rapidly exit their host cell when exposed to calcium ionophores. Calcium-dependent protein kinase 3 (*Tg*CDPK3) was previously identified as a key mediator in this process, as *Tg*CDPK3 knockout (Δ*cdpk3*) parasites fail to egress in a timely manner. Phosphoproteomic analysis comparing WT with Δ*cdpk3* parasites revealed changes in the *Tg*CDPK3-dependent phosphoproteome that included proteins important for regulating motility, but also metabolic enzymes, indicating that *Tg*CDPK3 controls processes beyond egress. Here we have investigated a predicted direct target of *Tg*CDPK3, ApiAT5-3, a putative transporter of the major facilitator superfamily, and show that it is rapidly phosphorylated at serine 56 after induction of calcium signalling. Conditional knockout of *apiAT5-3* results in transcriptional up-regulation of most ribosomal subunits, but no alternative transporters, and subsequent parasite death. Mutating the S56 to a non-phosphorylatable alanine leads to a fitness cost, suggesting that phosphorylation of this residue is beneficial, albeit not essential, for tyrosine import. Using a combination of metabolomics and heterologous expression, we confirmed a primary role in tyrosine import for ApiAT5-3. However, no significant differences in tyrosine import could be detected in phosphorylation site mutants showing that if tyrosine transport is affected by S56 phosphorylation, its regulatory role is subtle.

For Peer Review

Introduction

The fast growing tachyzoite stage of the protozoan parasite *Toxoplasma gondii* requires cycles of host cell invasion, replication, and lysis for its successful proliferation within the host. Each step of this lytic cycle involves tightly regulated signalling pathways, the intricacies of which remain largely unknown. Paramount to parasite survival is the ability to sense and respond to changes in the environment for which the divalent calcium ion (Ca^{2+}) acts as an important secondary messenger (Lourido and Moreno, 2015). Changes in free intracellular $[Ca^{2+}]_i$ levels, via release of Ca^{2+} from organellar Ca^{2+} stores, can be induced by the addition of Ca^{2+} ionophores, such as A23187 or phosphodiesterase inhibitors (Sidik et al., 2016a; Stewart et al., 2016). Ca^{2+} flux regulates key processes including secretion of micronemes prior to host cell entry (Carruthers and Sibley, 1999), parasite motility (Wetzel et al., 2004), and host cell egress (Endo et al., 1982) and invasion (Lovett and Sibley, 2003). Inversely, these processes can all be inhibited by Ca^{2+} immobilisers or chelators, such as BAPTA-AM (Black et al., 2000; Mondragon and Frixione, 1996; Moudy et al., 2001; Wetzel et al., 2004). Ca^{2+} release leads to the activation of Ca^{2+} binding proteins such as calmodulins, calcineurin B-like kinases and calcium-dependent protein kinases (CDPKs). *T. gondii* calcium-dependent protein kinase 3 (*Tg*CDPK3), for example, has been implicated in the regulation of ionophore induced egress, IIE (i.e. the rapid exit of tachyzoites from a host cell on addition of ionophore) and ionophore induced death, IID (i.e. the loss of infectivity of extracellular parasites after prolonged exposure to ionophore) (Black et al., 2000). *TgCDPK3* KO (Δ*cdpk3*) (McCoy et al., 2012), mutants (Black et al., 2000), and chemically inhibited *Tg*CDPK3 lines (Lourido

For Peer Review

et al., 2012) all show a deficiency in IIE and IID. *Tg*CDPK3 is a serine/threonine kinase belonging to a large family of CDPKs also found in plants and ciliates, but absent in humans. It is anchored to the parasite plasma membrane, via N-terminal myristoylation and palmitoylation motifs (Garrison et al., 2012; Lourido et al., 2012; McCoy et al., 2012), facing the lumen of the parasite. Like all CDPKs, *Tg*CDPK3 possesses a C-terminal calmodulin-like domain that consists of EF hands, known as the CDPK activation domain, as well as upstream autoinhibitory and catalytic domains (Billker et al., 2009; Huang et al., 1996). Binding of Ca^{2+} to the EF hands causes a structural rearrangement that frees up the active site of the kinase domain, allowing for substrate phosphorylation (Wernimont et al., 2010, 2011). A quantitative phosphoproteome study revealed 156 phosphorylation sites that are differentially phosphorylated between WT and *Tg*CDPK3 mutant parasites (Treeck et al., 2014). The *Tg*CDPK3-dependent phosphoproteome includes phosphorylation sites on proteins involved in parasite motility, such as the cyclase-associated protein and myosin A (Myo A), but also, and perhaps surprisingly, those involved in metabolic processes such as the α-ketoacid dehydrogenase (BCKDH) subunit, E1α, required for the breakdown of branched-chain amino acids (BCAAs) and conversion of pyruvate to the TCA driver acetyl-CoA (MacRae et al., 2012; Oppenheim et al., 2014). The link to proteins not obviously involved in egress and motility, as well as changes in the phosphoproteome regardless of the presence of ionophore, suggests that *Tg*CDPK3 function extends beyond egress.

The phosphorylation site that appeared to have one of the most marked reductions in phosphorylation state in *Tg*CDPK3 mutants compared to WT parasites (Treeck et

For Peer Review

al., 2014), is situated within a putative transporter of the MFS family (TGGT1_257530, named ApiAT5-3 as per (Parker et al., 2018)) that has moderate homology to a BCAA transporter. Given the additional evidence from the phosphoproteomic dataset that *Tg*CDPK3 putatively regulates BCAA catabolism via BCKDH, we hypothesised that *Tg*CDPK3 might be involved in BCAA uptake in addition to regulating motility. Through functional analysis we show that ApiAT5-3 is rapidly phosphorylated at serine 56 (S56) during the first minute of induced egress. Using a conditional KO approach, we show that ApiAT5-3 is essential, and that deletion leads to a delayed death phenotype that is accompanied by a transcriptional response relating to translational stress. Using a combination of metabolic analysis and heterologous expression in *Xenopus laevis* oocytes we confirm that ApiAT5-3 transports tyrosine but has only limited capacity to transport BCAAs. In growth competition assays performed with parasite lines that rely on phosphomutants or phosphomimetics, we show that phosphorylation of S56 may be important, but not essential, for parasite fitness. However, we could not measure significant differences in tyrosine import using metabolomic or heterologous expression assays of phosphorylation site mutants. This suggests that either *Tg*CDPK3 mediated phosphorylation is not important for ApiAT5-3 function, or that the effect is too subtle to measure and plays a small contribution to the phenotypes observed for *Tg*CDPK3 inactivation.

For Peer Review

Results

ApiAT5-3 is located at the parasite periphery and phosphorylated during ionophore induced egress in a *Tg*CDPK3-dependent manner.

ApiAT5-3 was previously identified as phosphorylated at serine 56 in a *Tg*CDPK3-dependent manner (Treeck et al., 2014). BLAST analysis using the Transporter Classification Database (http://www.tcdb.org/) predicts that ApiAT5-3 possesses a modest level of homology to a BCAA transporter. This was interesting, as deletion of *TgCDPK3* was previously shown to lead to upregulation of the BCKDH complex (Treeck et al., 2014), involved in BCAA catabolism. This indicated that *Tg*CDPK3 may directly control BCAA transport by phosphorylating ApiAT5-3.

Topology prediction (https://embnet.vital-it.ch/software/TMPRED_form.html (Hofmann, 1993)) places the N-terminal regions of ApiAT5-3 at the luminal side of the parasite, potentially allowing for direct interaction with *Tg*CDPK3, which also localises to the plasma membrane. ApiAT5-3 contains several phosphorylation sites at its N-terminus, of which S56 was the only one previously identified as being *Tg*CDPK3-dependent (Fig. 1A, upper panel). It is entirely plausible, however, that kinases other than *Tg*CDPK3 act during egress to phosphorylate additional residues on the ApiAT5-3 N-terminus. To investigate this, we queried a dataset recently generated in our laboratory in which we have quantified, using tandem-mass-tag technology (Thompson et al., 2003), phosphorylation site abundance on *T. gondii* proteins across 4 time points (0, 15, 30 and 60 s) following ionophore-treatment (Caia Dominicus, in preparation). From the ~850 phosphorylation sites that are

For Peer Review

phosphorylated or de-phosphorylated during egress, we identified S56 of ApiAT5-3 as increasingly phosphorylated over time (Fig. 1A, lower panel, S1 Table). We also identified several proteins already known to be more phosphorylated in response to Ca^{2+} signalling including Myosin A, Myosin F and DrpB (Lourido et al., 2013; Nebl et al., 2011; Treeck et al., 2014). None of the other phosphorylation sites on the ApiAT5-3 N-terminus increased in phosphorylation state prior to, or during egress (S1 Table). However, S15 of ApiAT5-3 was dephosphorylated during ionophore-treatment. Collectively these data indicate that S56 is phosphorylated in a *Tg*CDPK3-dependent manner upon Ca^{2+} stimulation, and that a phosphatase is acting on S15 during the same period, while the other phosphorylation sites either remain unaffected or are not detected by the assay.

To localise ApiAT5-3 in *T. gondii* parasites we introduced an ectopic copy of the *apiAT5-3* gene with a HA-epitope tag at its C-terminal, into RH Δ*hxgprt* parasites (ApiAT5-3::HA). 1000 bp upstream of the start-ATG were used as a predicted promotor to ensure natural expression levels. Western blotting confirmed expression of a 42 KDa protein close to the predicted size (56 KDa) (Fig. 1B). Immunofluorescence assays (IFA) showed ApiAT5-3 at the periphery of the parasite, co-localising with SAG1 that resides at the plasma membrane (Fig. 1C). No ApiAT5-3::HA could be detected in nascent daughter cells, a hallmark of most inner membrane complex proteins. Together, these data suggest that ApiAT5-3 localises, like *Tg*CDPK3, to the plasma membrane, and thus, could be a *bona fide* target of *Tg*CDPK3 *in vivo*.

For Peer Review

159

160 ***apiAT5-3* deletion causes delayed parasite death**

161 ApiAT5-3 depletion is predicted to have a high fitness cost (Toxo DB 7.1 (Sidik et al.,
162 2016b)). Accordingly, we generated a conditional KO using the dimerisable cre
163 recombinase (DiCre) strategy. We replaced the endogenous copy of *apiAT5-3* with a
164 recodonised version in RH Δ*ku80*^{DiCre} parasites, by double homologous
165 recombination, using a double-guide strategy (Long et al., 2016) (Fig. 2A). We initially
166 placed a loxP site adjacent to the Kozac sequence of ApiAT5-3 but were unable to
167 obtain correct integration. We hypothesised that the loxP sequence might be
168 interfering with promotor elements and moved it 100 and 200 bp upstream of the
169 predicted start ATG, respectively. Both of these constructs correctly integrated into
170 the genome. Subsequent analyses were performed with the resulting ApiAT5-3_loxP,
171 with the loxP at ATG -100bp. Integration was confirmed by PCR amplification (Fig.
172 2B, left panel). To test whether ApiAT5-3 is an essential gene we treated parasites for
173 4h with either rapamycin (RAP) or DMSO. PCR analysis showed a near complete
174 excision of the floxed gene (Fig. 2B, right panel). Correct excision of the ApiAT5-3
175 open reading frame resulted in YFP positive parasites that could be readily
176 distinguished from WT by microscopy (Fig. 2C). Upon performing plaque assays it
177 became evident that RAP, but not DMSO-treatment, resulted in a complete block in
178 plaque formation (Fig. 2D). A small number (<0.5%) of plaques could be identified in
179 RAP-treated cultures, however, parasites contained in these plaques where YFP(-),
180 indicating that they arose from non-excised parasites (data not shown). Over time
181 these non-excised parasites within the RAP-treated population outgrew the KOs (Fig.

For Peer Review

S1A), further reinforcing the fact that ApiAT5-3 is essential for parasite survival under these experimental conditions. These non-excising parasites (termed ApiAT5-3_loxP^{dDiCre}) were isolated and, even on the addition of subsequent RAP, did not lose their endogenous copy of the gene (Fig. S1B). These ApiAT5-3_loxP^{dDicre}, which presumably possess a non-functioning diCre recombinase, were used as controls for subsequent experiments, as detailed below. In an attempt to isolate *apiAT5-3* KOs and generate stable Δ*apiAT5-3* lines, YFP (+) parasites were sorted by flow cytometry. However, neither sorting for a population of excised, YFP (+) parasites using fluorescence-activated cell sorting (FACS), nor single-cell cloning by limiting dilution after RAP-mediated excision, resulted in viable parasites. Although small plaques in cloning plates were initially visible under the microscope after 9 days (Fig. S1C), they did not grow any further, suggesting that *apiAT5-3* KO leads to eventual parasite death rather than a maintenance of growth at low levels.

To visualise at which time points ApiAT5-3 is important, we followed replication of live RAP-treated ApiAT5-3_loxP parasites over 3 lytic cycles, where each lytic cycle is defined as growth over 36 hrs, before passage into a fresh culture dish containing host cells. This analysis revealed that in the first cycle, RAP-treated (*apiAT5-3* KO) parasite numbers and replication rate remained comparable to DMSO-treated (WT) parasites (Fig. 2E). However, by 36 hrs into the second replicative cycle there was a 60.7% decrease in the number of vacuoles with more than 16 parasites compared to the DMSO control. By the end of the 3rd cycle the *apiAT5-3* KO parasites consisted largely of 2 or fewer parasites/vacuole, even after the WT had successfully egressed

For Peer Review

(48 hrs into cycle). To better identify phenotypic consequences of *apiAT5-3* deletion, we followed replication over time using live-video microscopy. We started recording 29 hrs into the third lytic cycle post RAP-treatment, by which time *apiAT5-3* KO parasites display a marked growth defect. To facilitate a more accurate comparison between *apiAT5-3* KO and WT parasites, tdTomato expressing RH parasites (RH Tom) were spiked into the imaging wells at a 1:1 ratio. These analyses revealed that *apiAT5-3* KO does not lead to early egress. However, in the subsequent parasite cycle parasites that invade often do not proceed beyond 2 parasites/ vacuole (Fig. 2F, Movies S1A and B).

As we showed that ApiAT5-3 is phosphorylated directly after ionophore-treatment (Fig. 1A), we postulated that it may be required for IIE. To assess this, we performed egress assays of the DMSO- and RAP-treated lines in the presence of 8 µM Ca^{2+} ionophore. However, there was no significant difference between the KO and WT (Fig. 2G) suggesting that phosphorylation of ApiAT5-3, in response to elevated Ca^{2+} levels, plays a role in processes other than egress.

For Peer Review

apiAT5-3 deletion causes upregulation of genes encoding for ribosome subunits, but not alternative transporters

Deletion of a transporter may lead to up-regulation of alternative transporters or may manifest as a stress response that carries a detectable signature. To investigate this, we measured transcript levels using RNA-seq, comparing RAP-treated ApiAT5-3_loxP with ApiAT5-3_loxP^{dDiCre} parasites, which, as mentioned previously, do not excise the endogenous locus, even when treated with RAP (Fig. S1B). RNA was isolated in

biological triplicate at 4 hrs post RAP-treatment, the time point at which we did not expect to see major changes in the transcriptome, and 60 hrs post treatment, by which time point the RAP-treated ApiAT5-3_loxP parasites are still viable but start to display a growth defect. Indeed, at 4 hrs transcripts from the *apiAT5-3* gene were only slightly reduced in the RAP-treated ApiAT5-3_loxP parasites compared to the RAP-treated ApiAT5-3_loxP^{dDiCre} parasites (17.1%). In contrast, at 60 hrs post RAP-treatment, a 64.7% reduction was observed (Fig. 3A). Unexpectedly, only 435 transcripts showed a statistically significant differential expression between the WT and *apiAT5-3* KO parasites at the 60 hrs time point, compared to the 4 hrs time point, indicating a modest transcriptional response to *apiAT5-3* deletion (Fig. 3B). GO-term analysis of the differentially transcribed genes showed most enrichment (5.41-fold) for genes important for translation. Among this enriched group, these genes encode almost exclusively genes for ribosomal proteins (Fig. 3C, S2 Table). No single transporter was specifically up-regulated, indicating that there is no rapid transcriptional compensation when *apiAT5-3* is deleted.

Collectively these data show that ApiAT5-3 is an essential protein that is required for intracellular replication. Its depletion leads to a complete arrest in growth which is not accompanied by a substantial stress response, but rather modest signs of translational stress.

For Peer Review

Mutation of S56 to alanine, but not a phosphomimetic leads to a reduction in fitness.

Having established that ApiAT5-3 is essential for the lytic cycle, we next sought to examine the role of *Tg*CDPK3-mediated phosphorylation in ApiAT5-3 function. To do this, we complemented ApiAT5-3_loxP parasites with either WT ApiAT5-3, or variants where S56 is mutated to alanine (S56A) or to aspartic acid (S56D). To prevent possible differences in growth between the parasite lines due to differential expression of the complementation constructs, we inserted each into the *uprt* locus by double homologous recombination, under control of the endogenous promoter (Fig. 4A). Complementation into the *uprt* locus was verified by PCR (Fig. 4B). The complementation constructs also carried a C-terminal HA epitope tag to verify correct trafficking to the plasma membrane. Immunofluorescence displayed correct trafficking in all variants (Fig. 4C).

To compare fitness between the WT, the phosphomimetic (S56D), and the phosphomutant (S56A) complemented lines in the absence of *apiAT5-3*, we deleted the endogenous copy using RAP-treatment. This results in parasite strains that solely rely on the complemented copy of the gene. We confirmed correct excision of *apiAT5-3* by virtue of YFP expression post RAP-treatment (Fig. 4C) and PCR analysis (Fig. S2A). To ensure protein levels of the complemented genes were comparable, we attempted to quantify protein levels of the Δ*apiAT5-3*$^{\text{ApiAT5-3}}$, Δ*apiAT5-3*$^{\text{ApiAT5-3\_S56A}}$ and Δ*apiAT5-3*$^{\text{ApiAT5-3\_S56D}}$ lines by Western blot. However, despite several attempts we failed to visualize the complemented proteins. As an alternative approach we sought to quantify the protein levels using fluorescent anti-HA antibodies and

For Peer Review

analysis by flow cytometry. Comparison of the geometric mean of fluorescence indicated that the amount of ApiAT5-3, ApiAT5-3_S56A or ApiAT5-3_S56D protein did not differ significantly between the complemented lines (Fig. 4D). This would suggest that any subsequent phenotypes were a result of mutation of the S56 phosphorylation site and not differing *apiAT5-3* expression levels. RAP-treated parasite lines were viable and allowed us to isolate clones by limiting dilution, all of which restored growth in plaque assays (Fig. S2B). This shows that i) complementation of *apiAT5-3* by expression at the *uprt* locus fully restores ApiAT5-3 function and ii) that neither the introduction of phosphomimetics nor phosphomutants of S56 are lethal to parasite growth. This is not surprising as deletion of *Tg*CDPK3, the kinase putatively responsible for ApiAT5-3 phosphorylation during egress, does not lead to a severe growth phenotype. Accordingly, phosphomutants would not be expected to display drastic differences in growth. We therefore performed competition assays in which we compared growth of YFP expressing complementation lines that fully rely on the complementation variant for growth (Δ*apiAT5-3*$^{\text{ApiAT5-3/S56A/S56D}}$) mixed in a 1:1 ratio with their non-excised, colourless counterpart (ApiAT5-3$^{\text{ApiAT5-3/S56A/S56D}}$). Using the ratio of 4',6-diamidino-2-phenylindole (DAPI) stained parasites (DAPI labels the DNA of all parasites) and YFP expressing parasites (YFP is expressed only in the complementation lines) we followed growth over 14 days in biological triplicates. While Δ*apiAT5-3*$^{\text{ApiAT5-3}}$ parasites showed no difference in growth compared to their WT control, Δ*apiAT5-3*$^{\text{ApiAT5-3\_S56A}}$ was reduced by 84.0% after 14 days (Fig. 4E).

For Peer Review

Strikingly, Δ*apiAT5-3*$^{ApiAT5\text{-}3\_S56D}$ was not outcompeted and grew at similar levels to the WT control.

Collectively these data indicate that phosphorylation of S56 while not essential is important for intracellular growth. However, we cannot exclude that mutating S56 to an alanine impacts protein function by other means than mimicking non-phosphorylated S56.

ApiAT5-3 is a primary transporter of tyrosine, but not branched-chain amino acids

The predicted homology of ApiAT5-3 to a BCAA transporter and the profound up-regulation of the BCKDH complex in Δ*cdpk3* parasites suggested a direct role for ApiAT5-3 in BCAA transport. To test this, we expressed *apiAT5-3* in the heterologous expression system, *X. laevis* oocytes. Concurrently with our study, data were presented that ApiAT5-3 may be a tyrosine transporter (Giel van Dooren, personal communication and pre-published in BioRx (Parker et al., 2018)). We therefore tested BCAA import and replicated the tyrosine uptake capacity of ApiAT5-3 in oocytes expressing WT ApiAT5-3 (Fig. 5A). Measuring unidirectional influx, we observed a significant (4.0-fold) increase in the uptake of ^{14}C-tyrosine into ApiAT5-3-expressing oocytes compared to either water-injected or uninjected control oocytes under the conditions tested, consistent with results from (Parker et al., 2018). We also observed moderate ApiAT5-3-dependent phenylalanine influx, but not for the

For Peer Review

316 BCAA valine (Fig. S3A), suggesting that, while ApiAT5-3 is capable of tyrosine
317 transport, it is unlikely to be a major BCAA transporter.

318 To verify the role of ApiAT5-3 in tyrosine transport in our conditional KO parasites,
319 we measured intracellular ^{13}C-tyrosine levels in RAP-treated Δ*apiAT5-3*$^{ApiAT5-3}$ (WT)
320 and ApiAT5-3_loxP (KO) parasites (74 hrs post excision), after 1 hr in the presence of
321 growth media containing ^{13}C-tyrosine. In an analogous manner, we also measured
322 ^{13}C-isoleucine uptake in order to verify if ApiAT5-3 is also a BCAA transporter.
323 Δ*apiAT5-3*$^{ApiAT5-3}$ was used instead of DMSO-treated ApiAT5-3_loxP to control for any
324 potential effects of RAP on parasite metabolism. This analysis verified a reduction of
325 ^{13}C-labelled tyrosine uptake (40.5% compared to *ΔapiAT5-3*$^{ApiAT5-3}$), but not
326 isoleucine uptake (4.3% compared to *ΔapiAT5-3*$^{ApiAT5-3}$) (Fig. 5B). We also measured
327 the intracellular abundance of all detectable amino acids when labelling with ^{13}C-
328 tyrosine. We observed a reduction of intracellular tyrosine abundance (63.2%) in the
329 *apiAT5-3* KO cells (as expected), but not phenylalanine which was slightly increased
330 in relative abundance (17.45%), suggesting that while ApiAT5-3 is able to transport
331 phenylalanine in oocytes, it is not the major phenylalanine transporter in *T. gondii*
332 (Fig. S3B). It is important to note that our metabolome analysis was performed at the
333 end of cycle 2 after RAP-treatment, when RAP-treated apiAT5-3_loxP parasites are
334 still viable but start to display a reduction of growth (Fig. 2E). Therefore, we predict
335 that low levels of ApiAT5-3 present at this stage are responsible for the residual
336 transport of tyrosine. Interestingly, we also observed a reduction in intracellular
337 aspartate (38.5%) and glycine (28.3%) in *apiAT5-3* KO cells (Fig. S3B). Since *T. gondii*
338 is not known to be auxotrophic for these amino acids we reasoned that the observed

For Peer Review

death phenotype is unlikely caused by a defect in glycine or aspartate import, and instead focussed our subsequent analysis on tyrosine. We also observed an increase in the abundance of glutamine, valine, isoleucine and proline, indicating potential wider metabolic effects.

To test whether exogenous tyrosine can complement the loss of ApiAT5-3 we grew parasites in media with 5× the normal amount of tyrosine (2 mM). However, plaque assays revealed that RAP treated ApiAT5-3_loxP parasite growth was not restored (Fig. 5C). Several attempts were also made to isolate stable Δ*apiAT5-3* clonal lines by limiting dilution in the presence of 2 mM tyrosine. Again however, this was unsuccessful as parasites appeared to die after several rounds of replication, much like those grown in normal media. In other organisms, phenylalanine can be converted into tyrosine. Therefore, we tested whether phenylalanine supplementation (2 mM) can rescue the growth phenotype of *apiAT5-3* KO parasites. No growth rescue could be observed (Fig. S3D). Together, these results suggest that ApiAT5-3 is the only transporter of tyrosine in *T. gondii* and that phenylalanine cannot be readily converted into tyrosine in *T. gondii* parasites.

As ApiAT5-3 is phosphorylated during egress in a *Tg*CDPK3-dependent manner, and as S56 phosphomutants display a moderate fitness cost, we postulated a functional link between S56 phosphorylation and tyrosine import. We therefore tested uptake of isotopically labelled tyrosine by extracellular Δ*apiAT5-3*$^{\text{ApiAT5-3\_S56A}}$ and Δ*apiAT5-3*$^{\text{ApiAT5-3\_S56D}}$ phosphomutant strains. No statistically significant difference in tyrosine

For Peer Review

import was observed in these assays (Fig. S3E) either because phosphorylation of S56 plays no role in tyrosine import, or because the effect of phosphomutations on tyrosine import at the parasite level is subtle. Therefore, we also assessed differences in tyrosine uptake in *X. laevis* oocytes heterologously expressing ApiAT5-3_S56A and ApiAT5-3_S56D. As it has not been determined whether the S56 residue is phosphorylated *in situ* by native oocyte kinases, it is difficult to determine the exact role of phosphorylation in the tyrosine transport function of ApiAT5-3 expressing oocytes. However, comparison between S56A phospho-null to S56D phosphomimic expressing oocytes could provide a good indication as to the functional relevance of this residue. Although ApiAT5-3_S56A-expressing oocytes displayed a trend towards a reduction in tyrosine uptake (average 19.5% reduction in S56A relative to WT ApiAT5-3-expressing oocytes), this difference was not statistically significant (Fig. S3F). The S56D expressing oocytes display a marginal increase in tyrosine uptake of 14.0%, that again was not statistically significant. Collectively these data indicate that ApiAT5-3 is a primary tyrosine transporter and that S56 phosphorylation plays only a minor, if any, role in tyrosine import.

Discussion

*Tg*CDPK3 has previously been implicated in controlling distinct biological processes such as gliding motility and metabolism. How these are linked, however, has been unclear. Mutants that display only IIE and IID phenotypes have been identified (Black et al., 2000; Gaji et al., 2015), arguing that *Tg*CDPK3 may be an upstream regulator of both processes. Here we show that upon activation by the Ca^{2+} ionophore A23187, *Tg*CDPK3 leads to an increase in ApiAT5-3 phosphorylation at S56. This occurs at the

For Peer Review

same time, and to a similar intensity, as other previously identified targets of *Tg*CDPK3 (e.g. serine 21/22 of MyoA) and other kinases involved in signalling (e.g. *Tg*CDPK1). MyoA and ApiAT5-3 are both located at, or close to, the plasma membrane. It is conceivable that, upon activation, *Tg*CDPK3 phosphorylates proteins at the plasma membrane, some of which are important for motility and others (e.g. transporters) that prepare the parasite for the extracellular milieu. In this study we demonstrate that the S56 residue becomes rapidly phosphorylated prior to egress in a *Tg*CDPK3-dependent manner. However, the timing of phosphorylation during egress does not a appear to be linked to the phenotype of the ApiAT5-3 KO, which stalls growth after invasion of the host cell. The timing of phosphorylation during egress and an apparent role of the transporter during intracellular growth could be explained that phosphorylation prepares the parasite for the extracellular milieu, or for reinvasion. Interestingly, ApiAT5-3 possesses several other phosphorylation sites in its N-terminus, aside from S56, that either do not change in phosphorylation state or, in the case of S15, appear dephosphorylated during induced Ca^{2+} signalling. How S15 dephosphorylation and S56 phosphorylation are controlling ApiAT5-3 function requires further investigation, however it is evident that mutating S56 to a non-phosphorylatable residue markedly reduces parasite fitness, similar to the growth defect observed for *Tg*CDPK3 mutants (McCoy et al., 2012). Phosphorylation of transporters has been shown to regulate affinity, specificity and flux of cargo (Aryal et al., 2015; Jang et al., 2014; Lee et al., 2007; Liu and Tsay, 2003; Ramamoorthy et al., 2010; Tamura et al., 2013). Accordingly, the observed fitness cost in S56A mutants could be indicative of a reduction in tyrosine import, for which the parasite is

For Peer Review

auxotrophic (Marino and Boothroyd, 2017). It appears that deletion of ApiAT5-3 has little effect during the first two lytic cycles of division, indicating that relatively normal growth rates can be sustained with lower ApiAT5-3 levels. A critical point is reached between the 2nd and 3rd lytic cycles, when parasites are still able to egress, but then fail to develop beyond 2 parasites/ vacuole in most cases. Whether this is because ApiAT5-3 function is critically important shortly after invasion, or whether this is the point at which ApiAT5-3 protein levels are diluted below a critical concentration is not known and further work will be required to answer this question.

While we observed a clear role for ApiAT5-3 in tyrosine transport, expression of the ApiAT5_S56A phosphomutant did not lead to significant changes in tyrosine import in *Toxoplasma* parasites or in *Xenopus* oocytes. Although a small reduction in tyrosine import was observed in *Xenopus* oocytes expressing ApiAT5-3_S56A, the difference is subtle and could be the result of small differences in expression levels or phosphorylation state of ApiAT5-3 in oocytes. Thus, the oocyte assays did not allow us to draw conclusions on the effect of S56 phosphorylation, apart from that it appears not to be a prerequisite for tyrosine import in *T. gondii*. Whether or not S56 phosphorylation plays a minor role in regulating ApiAT5-3 cannot be answered at this stage. Growth competition assays showed that a phosphomimetic mutant gives parasites a competitive growth benefit. While this could be a result of changing a functionally important residue to a non-related amino acid, it could also be that phosphorylation of S56 plays a small role in ApiAT5-3 regulation. We observed an 84.0% reduction in growth of Δ*apiAT5-3*$^{\text{ApiAT5-3\_S56A}}$ mutants compared to WT

For Peer Review

parasites over 14 days. This translates into a reduced replication rate of 6.74% per 24 hrs. If this growth defect is a direct result of reduced tyrosine import, we would predict there to only be a 0.56% reduction in import during the 1 hr period in which the ^{13}C-tyrosine uptake assays are performed. This difference would be too small to measure with the methods available. The observation that tyrosine transport by ApiAT5-3 appears only marginally affected by *Tg*CDPK3 activity, leaves open the question as to how *Tg*CDPK3 is linked to the changes observed on the phosphoproteome of metabolic enzymes in *Tg*CDPK3 mutants (Treeck et al., 2014). Further work is required to answer this question.

Apart from regulating amino acid transport, phosphorylation of transporters has also been shown to regulate trafficking to the surface (Abramian et al., 2014; Nissen-Meyer et al., 2011; Rice et al., 2012). However, a role for S56 in trafficking is less likely for two reasons: i) we did not observe any obvious defects in surface translocation of the transporter in parasites and ii) *Tg*CDPK3 phosphorylates S56 shortly before, or during egress, at which state the transporter is already on the surface. If S56 phosphorylation was important for surface translocation, we would expect this to occur at an earlier stage. However, we cannot exclude the possibility that minor differences in trafficking capacity impact tyrosine transport, resulting in the growth phenotype.

Interestingly we haven't been able to rescue the effect of *apiAT5-3* loss in our conditional KO parasites through growth in high tyrosine concentrations. These results differ from those in Parker, et al. whereby growth can, at least partially, be rescued in high tyrosine medium (Parker et al., 2018). One mechanism to counter low

For Peer Review

tyrosine levels that most organisms possess, is the ability to convert phenylalanine into tyrosine, via the enzyme phenylalanine-4-hydroxylase (AAH). However, the inability to overcome the tyrosine import related growth defect in ApiAT5-3 conditional KOs through addition of exogenous phenylalanine, indicates that this pathway is not available. Indeed, both isoforms of AAH (AAH1 and AAH2) have recently been shown to be secreted into the host cell during *Toxoplasma* infection, where they would be unable to rescue a tyrosine transporter defect in the plasma membrane (Marino and Boothroyd, 2017; Wang et al., 2017). Another explanation as to why Parker, et al. have successfully rescued the effects of *apiAP5-3* deletion through addition of excess tyrosine, could be via the upregulation of alternative transporters. Although a small amount of tyrosine appears to be imported in our *apiAT5-3* KO line (Fig. 5B), this is likely due to the presence of residual ApiAT5-3 protein in the plasma membrane after RAP-treatment. Along with our inability to rescue growth upon tyrosine supplementation, we conclude that this residual tyrosine import is unlikely due to an alternative transporter. Further to this, our transcriptomic analysis argues against a rapid sensing and transcriptional compensation for the lack of tyrosine import, so if upregulation of alternative transporters occurs, it will be a slow process. Another explanation may be that slight differences in the genetic background or passage history, and potential epigenetic changes in the parental strains, leads to a difference in capacity for amino acid transport. There is some indication that this may be the case as, in our metabolomics experiments, the ApiAT5-3 deletion showed reduced levels of glycine and aspartic acid in addition to tyrosine, while in Parker, et al., other amino acids were observed

For Peer Review

to be less abundant in addition to tyrosine. We also saw an increase in abundance of some amino acids that differ from Parker, K *et al.* It may be interesting in the future, to compare our *apiAT5-3* KO with that of Parker, et al. and identify any compensatory mechanisms the parasites can use to adjust to tyrosine starvation. Interestingly, deletion of *apiAT5-3* leads to a growth arrest that is not accompanied by major transcriptional responses, but up-regulation of most transcripts for ribosomal subunits, which indicate translational changes in response to tyrosine depletion. We have not further pursued this response in this study, but it is reminiscent of the hibernation state in *Plasmodium falciparum*, whereby depletion of isoleucine, an essential amino acid for this parasite, leads to arrest in growth by translational arrest without a major stress response (Babbitt et al., 2012). This would suggest that translational arrest may be a common response among apicomplexan parasites during amino acid starvation.

In summary we show that ApiAT5-3, a novel *T. gondii* tyrosine transporter, is rapidly phosphorylated in a *Tg*CDPK3 dependent manner at S56 prior to, and during egress from the host cell. This *Tg*CDPK3-dependent phosphorylation at S56 appears important for parasite fitness based on phosphomimetics and phosphomutants. These results, together with previous studies, support the notion that *Tg*CDPK3 simultaneously targets several proteins in, or at, the plasma membrane that are implicated in divergent biological processes, such as motility and nutrient homeostasis. If the phosphorylation sites that depend on *Tg*CDPK3 function each play a small functional role in *T. gondii* biology, as implicated for S56 on ApiAT5-3, the

For Peer Review

phenotypes observed in Δ*cdpk3* parasites may be an accumulation of effects on various proteins, which is likely true for other kinases as well.

Experimental procedures

Parasite culture

T. gondii parasites were cultured in a confluent monolayer of human foreskin fibroblasts (HFFs) maintained in Dulbecco's Modified Eagle Medium (DMEM), GlutaMAX supplemented with 10% foetal bovine serum, at 37°C and 5% CO_2.

Plasmid and parasite strain generation

A comprehensive list of primers and parasite lines used throughout this study are described in S3 and S4 Tables respectively. To generate the epitope tagged ApiAT5-3::HA line, the *apiAT5-3* gene and associated 5' UTR were PCR-amplified from RH *T. gondii* gDNA using the primers 1 and 2 and cloned using Gibson assembly (Gibson et al., 2008) into pGRA::HA::HPT (Saeij et al., 2006), linearised with HindIII and NcoI. 25 µg of the pGRA::ApiAT5-3::HA vector was transfected into RH *Δhxgprt* parasites as previously described (Soldati and Boothroyd, 1993). 16-20 hrs after transfection, transgenic parasites were selected using 25 µM mycophenolic acid (MPA) and 50 µg/ml xanthine (XAN). To generate the ApiAT5-3_loxP conditional KO lines, the *apiAT5-3* 5'UTR was first PCR-amplified from gDNA with primers 3 and 4. This PCR product was inserted, along with the synthetic DNA constructs *loxP_apiAT5-3_loxP_yfp* and *loxP*(-100)*_apiAT5-3* (see S3 Table for full sequences), by Gibson assembly into pG140::Actin::YFP (Andenmatten et al., 2013) that had been PCR-amplified using primers 5 and 6 to remove the actin gene. 2 µg of the subsequent

For Peer Review

pG140::ApiAT5-3_loxP::YFP plasmid was linearised with ScaI and co-transfected into RH *Δku80Δhxgprt* with pSag1::Cas9-U6::dbl-sgApiAT5-3, in a molar ratio of 1:10. The pSag1::Cas9-U6::dbl-sgApiAT5-3 vector was generated by PCR-amplification of the pSag1::Cas9-U6 (Shen et al., 2014) vector using primers 7 and 8 to insert the 5' gRNA (gRNA 1) and 9 and 8 to insert the 3' gRNA (gRNA 2), prior to re-ligation with T4 DNA Ligase (New England Biolabs). gRNA 1 was then amplified using primers 10 and 11 and Gibson cloned into the pSag1::Cas9-U6::sg2ApiAT5-3 that had been linearised with KpnI and XhoI as per (Long et al., 2016). Transgenic parasites were selected using MPA/XAN as described for pGRA::ApiAT5-3::HA. 5' and 3' integration was confirmed using primer pairs 12 and 13, and 14 and 15 respectively. Absence of WT *apiAT5-3* was confirmed using primers 16 and 17. DiCre-mediated *apiAT5-3* excision was induced with the addition of 50 nM RAP to ApiAT5-3_loxP parasites for 4 hrs. Excision was confirmed using primers 13 and 16. To introduce an ectopic copy of *apiAT5-3* into the *uprt* gene locus, the *apiAT5-3* gene, and associated 5' UTR, were PCR-amplified from gDNA using primers 18 and 19 which was then inserted into the BamHI/ PacI digested pUPRT::DHFR-D vector (Addgene plasmid #58258 (Shen et al., 2014)) using Gibson assembly. To generate the pUPRT::ApiAT5-3_S56A::HA and pUPRT::ApiAT5-3_S56D::HA vectors, the pUPRT::ApiAT5-3::HA vector was modified by site directed mutagenesis using the primers 20 and 21 (S56A) or 22 (S56D). pUPRT::ApiAT5-3::HA, pUPRT::ApiAT5-3_S56A::HA and pUPRT::ApiAT5-3_S56D::HA were linearised with PciI prior to the co-transfection of 2 µg into RH *Δku80Δhxgprt* ApiAT5-3_loxP with pSag1::Cas9-U6::sgUPRT (Addgene plasmid #54467 (Shen et al., 2014)) in a molar ratio of 1:10. Transgenic parasites were selected by the addition of

For Peer Review

5 µM 5'-fluo-2'-deoxyuridine to culture medium, 16-20 hrs post-transfection. Integration into the genome was confirmed using primer pairs 23 and 24, and 25 and 26 respectively. Absence of *uprt* was confirmed using primers 27 and 28.

Western blotting and immunofluorescent imaging

For Western blot analysis, intracellular parasites were lysed in Laemmli buffer (60 mM Tris-HCl pH6.8, 1% SDS, 5% glycerol, 5% b-mercaptoethanol, 0.01% bromophenol blue) and heated to 37°C for 30 mins prior to separation on a 10% sodium dodecyl-polyacrylamide gel. Proteins were transferred onto a nitrocellulose membrane prior to blocking in 3% milk, 0.1% Tween-20 PBS. HA-tagged ApiAT5-3 was detected using rat anti-HA (1:500), followed by goat anti-rat LI-COR secondary antibody (1:1500) and visualised with a LI-COR Odyssey scanner. Loading control visualised with Abcam mouse anti-Toxo (1:1000), followed by goat anti-mouse LI-COR secondary antibody (1:1500).

IFA's were performed on intracellular parasites grown in HFFs on glass coverslips. 1×10^5 parasites were seeded 24 hrs prior to fixation with 3% formaldehyde (FA). PBS 0.1% Triton X-100 was added to the fixed cells for 10 mins prior to blocking with 3% bovine serum albumin in PBS for 1 hr. ApiAT5-3::HA was visualised using rat anti-HA (1:500) followed by addition of Alexa594 conjugated donkey anti-rat secondary antibody (1:2000). SAG1 visualised with mouse anti-SAG1 (1:1000) and Alexa488 conjugated donkey anti-rat secondary antibody (1:2000). DAPI, 5 µg/ml.

Plaque assay and amino acid complementation

For plaque assay analysis, 150 parasites were seeded on confluent HFF monolayers, grown in 24-well plates, and left undisturbed for 5 days, before fixing with chilled

For Peer Review

methanol and staining with 0.1% crystal violet. To assess growth in excess tyrosine, plaque assays were repeated either at normal tyrosine levels (400 µM L-tyrosine disodium salt; as per Gibco manufacturer) or in DMEM supplemented with 2mM L-tyrosine disodium salt (dissolved for 1 hour at 50 °C). To ensure tyrosine had successfully dissolved samples of the media were analysed by GC-MS as previously described (MacRae et al., 2012).

Replication assay

2×10^4 ApiAT5-3_loxP parasites were seeded in triplicate on confluent HFFs in both culture flasks and glass bottom 8-well imaging plates and left to invade for 1 hour prior to treatment with 50 nM RAP or equivalent volume DMSO, for 4 hrs. Parasites were imaged at 24, 36 and/or 48 hrs and split at 36 hrs into new flasks and imaging wells for the subsequent replication cycle. At each time point parasites were fixed in 3% FA and imaged on a Nikon Eclipse Ti-U inverted fluorescent microscope. Parasites/vacuole were counted manually from 5 fields of view at 20× magnification using the Nikon NIS-Elements software.

Live cell microscopy

ApiAT5-3_loxP parasites were treated with RAP or DMSO as previously described. 36 hrs into cycle 2 post RAP-treatment parasites were syringe lysed and seeded in glass bottom, 8-well imaging plates in a 1:1 ratio with RH Tom parasites. After a further 29 hrs, live parasites were imaged on a Nikon Eclipse Ti-U inverted fluorescent microscope every 30 mins for the next 30 hrs, in a temperature-controlled chamber at 37 °C and 5% CO_2. Images were analysed using the Nikon NIS-Elements software.

For Peer Review

Ionophore induced egress assays

ApiAT5-3_loxP parasites were seeded in 96-well imaging plates at a MOI of 0.5, 36 hrs post RAP/DMSO-treatment. IIE assays were performed in triplicate at 37 °C in Ringers buffer (155 mM NaCl, 3 mM KCl, 2 mM $CaCl_2$, 1 mM $MgCl_2$, 3 mM NaH_2PO_4, 10 mM HEPES, 10 mM glucose) 30 hrs later. The parasites were incubated with 8 µM Ca^{2+} ionophore A23187 for 0, 0.5, 1, 1.5, 2, 2.5, 3, 3.5, 4 and 5 mins prior to the addition of 16% FA to a final concentration of 3% for 15 mins. Wells were subsequently washed with PBS and stained with 5 µg/ml DAPI. Automated image acquisition of 25 fields per well was performed on a Cellomics Array Scan VTI HCS reader (Thermo Scientific) using a 20× objective. Image analysis was performed using the Compartmental Analysis BioApplication on HCS Studio (Thermo Scientific).

Competition assays and flow cytometry

For expression analysis of complemented lines, syringe lysed ApiAT5-3_loxP, Δ*apiAT5-3*$^{\text{ApiAT5-3}}$, Δ*apiAT5-3*$^{\text{ApiAT5-3\_S56A}}$ and Δ*apiAT5-3*$^{\text{ApiAT5-3\_S56D}}$ lines were spun at 72 × g to remove host cell debris for 1 min. The supernatant was spun at 2049 × g for 5 mins and the pellet fixed for 10 mins in 3% FA. Fixed parasites were washed in PBS and resuspended in 0.1 % Triton X-100 for 5 mins prior to staining with anti-HA conjugated to allophycocyanin (1:500) for 1 hr. The sample was washed and resuspended in PBS before running on a flow cytometer. For competition assays, 5×10^6 ApiAT5-3$^{\text{ApiAT5-3}}$, ApiAT5-3$^{\text{ApiAT5-3_S56A}}$ and ApiAT5-3$^{\text{ApiAT5-3_S56D}}$ parasites were mixed in a 1:1 ratio with Δ*apiAT5-3*$^{\text{ApiAT5-3}}$, Δ*apiAT5-3*$^{\text{ApiAT5-3\_S56A}}$ and Δ*apiAT5-3*$^{\text{ApiAT5-3\_S56D}}$ respectively. 5×10^4 parasites were added to fresh HFF monolayers prior to washing and fixation, as described previously. After fixation, parasites were stained

For Peer Review

with 5 µg/ml DAPI for 10 mins and washed and resuspended in PBS before running on a flow cytometer. All parasites were gated on DAPI fluorescence to prevent results being skewed by remaining unstained host cell debris. The proportion of DAPI (+); YFP (+) (representing Δ*apiAT5-3*$^{\text{ApiAT5-3/S56A/S56D}}$) compared to DAPI (+); YFP (-) (representing ApiAT5-3$^{\text{ApiAT5-3/S56A/S56D}}$) was calculated. The process was repeated 14 days later for comparison to day 0.

Oocyte maintenance and radiotracer uptake assays

ApiAT5-3, ApiAT5-3_S56A and ApiAT5-3_S56D were PCR amplified from Δ*apiAT5-3*$^{\text{ApiAT5-3}}$, Δ*apiAT5-3*$^{\text{ApiAT5-3\_S56A}}$ and Δ*apiAT5-3*$^{\text{ApiAT5-3\_S56D}}$ cDNA, respectively, using primers 29 and 30 to add a region of homology to the XkbN plasmid at the 5' end and a HA tag to the 3' end of each gene. These fragments were then amplified with primers 31 and 32 to add a 3' XkbN homology overhang. These resulting fragments were inserted by Gibson assembly into the XkbN1_*Pf*HT (a version of pSPGT1 (Woodrow et al., 1999) with a NotI site added to the MCS, provided by Ksenija Slavic) which had been digested with BglII and NotI, to remove the *Pf*HT gene. The resulting XkbN_ApiAT5-3, XkbN_ApiAT5-3_S56A and XkbN_ApiAT5-3 _S56D plasmids were linearised with XbaI for in vitro transcription using the Thermo Fisher mMessage mMachine transcription kit. Stage V to VI defolliculated *X. laevis* oocytes were obtained commercially (Ecocyte Biosciences) for subsequent functional transport studies. Oocytes were microinjected with cRNA (20 to 40 ng in 30 nl of water) encoding *apiAT5-3* template or with a comparable amount of diethylpyrocarbonate-treated water. The oocytes were maintained at 18 °C in oocyte Ringer 2 buffer (82.5 mM NaCl, 2.5 mM KCl, 1.5 mM $CaCl_2$, 1mM Na_2HPO_4, 1 mM $MgCl_2$ and 5 mM HEPES)

For Peer Review

637 and used for transport studies 72 hrs after cRNA injection. Transport measurements
638 were performed at room temperature on groups of 10 oocytes in ND96 medium (96
639 mM NaCl, 2 mM KCl, 2 mM $CaCl_2$, 1 mM $MgCl_2$ and 5 mM HEPES) containing 1 µM
640 radiolabelled U-^{14}C-L-tyrosine (specific activity of 486 mCi/mmol; Perkin Elmer), U-
641 ^{14}C-L-phenylalanine (specific activity of 508 mCi/mmol; Perkin Elmer) or U-^{14}C-L-
642 valine (specific activity of 271 mCi/mmol; Perkin Elmer). Transport was measured
643 at 10 min, over which time uptake of L-tyrosine is linear (Parker et al., 2018). Each
644 result was confirmed by at least 3 independent experiments.

645 **Metabolite labelling and extraction**

646 ApiAT5-3_loxP, Δ*apiAT5-3*$^{\text{ApiAT5-3}}$, Δ*apiAT5-3*$^{\text{ApiAT5-3\_S56A}}$ and Δ*apiAT5-3*$^{\text{ApiAT5-3\_S56D}}$
647 parasites were treated in triplicate with 50 nM RAP and, at the end of the first cycle,
648 seeded in 15 cm culture flasks. Stable isotope labelling (1 hr) of extracellular parasites
649 with 0.8 mM U-^{13}C-L-tyrosine or 4 mM U-^{13}C-L-isoleucine, metabolite extraction and
650 subsequent GC-MS analysis were all performed as per (MacRae et al., 2012), on an
651 Agilent GC-MSD (7890B-5977A). Data analysis was carried out using GAVIN software
652 (Behrends et al., 2011).

653 **RNA sequencing analysis**

654 *T. gondii* RNA was extracted as per the Qiagen RNA-easy mini kit user handbook
655 (#74104) from ~5×10^6 ApiAT5-3_loxP or ApiAT5-3_loxP$^{\text{dDiCre}}$ parasites at 0, 4 and 60
656 hrs post RAP-treatment. Analysis was performed in triplicate. The FASTQ files were
657 aligned using Bowtie 2 (Langmead and Salzberg, 2012) to Ensembl Protist release 35
658 of *T. gondii* (ToxoDB-7.1). They were then quantified using RSEM before being
659 processed using Bioconducor (Huber et al., 2015). We used DESeq2 (Love et al.,

For Peer Review

2014) to account for gene length and library size, and to test for the interaction between treatment and time point to generate the differential genelist. We corrected for multiple testing using the Benjamini-Hochberg procedure for false discovery rates. To validate the recodonised transcript, we both re-aligned to a custom genome rebuilt to include the novel sequence, and also used a pseudo-alignment approach to quantify purely the reads associated with the novel sequence (Bray et al., 2016).

Acknowledgements

We thank all members of the Treeck laboratory for critical discussions. We thank Giel Van Dooren and Sebastian Lourido for sharing unpublished data. We thank members of the following Science Technology platforms at the Francis Crick Institute: Bioinformatics, Advanced Sequencing, Peptide Synthesis, Proteomics and Flow Cytometry. This work was supported by awards to MT by the United States Institute of Health (NIH-R01AI123457) and The Francis Crick Institute (https://www.crick.ac.uk/), which receives its core funding from Cancer Research UK (FC001189; https://www.cancerresearchuk.org), the UK Medical Research Council (FC001189; https://www.mrc.ac.uk/) and the Wellcome Trust (FC001189; https://wellcome.ac.uk/). HMS is supported by the Wellcome Trust Institutional Strategic Support Fund (204809/Z/16/Z) awarded to St. George's University of London.

For Peer Review

Author contributions

BAW and MT conceived experiments and wrote the paper. BAW, CSD and MB designed and performed experiments and data analysis. NL performed experiments and data analysis. JIM and HMS helped conceive experiments and edited the paper.

References

Abramian, A.M., Comenencia-Ortiz, E., Modgil, A., Vien, T.N., Nakamura, Y., Moore, Y.E., Maguire, J.L., Terunuma, M., Davies, P.A., and Moss, S.J. (2014). Neurosteroids promote phosphorylation and membrane insertion of extrasynaptic GABAA receptors. PNAS *111*, 7132–7137.

Andenmatten, N., Egarter, S., Jackson, A.J., Jullien, N., Herman, J.-P., and Meissner, M. (2013). Conditional genome engineering in Toxoplasma gondii uncovers alternative invasion mechanisms. Nature Methods *10*, 125–127.

Aryal, B., Laurent, C., and Geisler, M. (2015). Learning from each other: ABC transporter regulation by protein phosphorylation in plant and mammalian systems. Biochemical Society Transactions *43*, 966–974.

Babbitt, S.E., Altenhofen, L., Cobbold, S.A., Istvan, E.S., Fennell, C., Doerig, C., Llinás, M., and Goldberg, D.E. (2012). Plasmodium falciparum responds to amino acid starvation by entering into a hibernatory state. PNAS *109*, E3278–E3287.

Behrends, V., Tredwell, G.D., and Bundy, J.G. (2011). A software complement to AMDIS for processing GC-MS metabolomic data. Anal. Biochem. *415*, 206–208.

Billker, O., Lourido, S., and Sibley, L.D. (2009). Calcium-Dependent Signaling and Kinases in Apicomplexan Parasites. Cell Host & Microbe *5*, 612–622.

Black, M.W., Arrizabalaga, G., and Boothroyd, J.C. (2000). Ionophore-resistant mutants of Toxoplasma gondii reveal host cell permeabilization as an early event in egress. Molecular and Cellular Biology *20*, 9399–9408.

Bray, N.L., Pimentel, H., Melsted, P., and Pachter, L. (2016). Near-optimal probabilistic RNA-seq quantification. Nat Biotechnol *34*, 525–527.

Carruthers, V.B., and Sibley, L.D. (1999). Mobilization of intracellular calcium stimulates microneme discharge in Toxoplasma gondii. Molecular Microbiology *31*, 421–428.

For Peer Review

712 Endo, T., Sethi, K.K., and Piekarski, G. (1982). Toxoplasma gondii: calcium ionophore
713 A23187-mediated exit of trophozoites from infected murine macrophages.
714 Experimental Parasitology *53*, 179–188.

715 Gaji, R.Y., Johnson, D.E., Treeck, M., Wang, M., Hudmon, A., and Arrizabalaga, G. (2015).
716 Phosphorylation of a Myosin Motor by TgCDPK3 Facilitates Rapid Initiation of
717 Motility during Toxoplasma gondii egress. PLoS Pathogens *11*, e1005268.

718 Garrison, E., Treeck, M., Ehret, E., Butz, H., Garbuz, T., Oswald, B.P., Settles, M.,
719 Boothroyd, J., and Arrizabalaga, G. (2012). A Forward Genetic Screen Reveals that
720 Calcium-dependent Protein Kinase 3 Regulates Egress in Toxoplasma. PLoS
721 Pathogens *8*, e1003049.

722 Gibson, D.G., Benders, G.A., Andrews-Pfannkoch, C., Denisova, E.A., Baden-Tillson, H.,
723 Zaveri, J., Stockwell, T.B., Brownley, A., Thomas, D.W., Algire, M.A., et al. (2008).
724 Complete chemical synthesis, assembly, and cloning of a Mycoplasma genitalium
725 genome. Science *319*, 1215–1220.

726 Hofmann (1993). TMbase - A database of membrane spanning proteins segments.
727 Biol. Chem. Hoppe-Seyler *374*.

728 Huang, J.F., Teyton, L., and Harper, J.F. (1996). Activation of a Ca2+-dependent protein
729 kinase involves intramolecular binding of a calmodulin-like regulatory domain.
730 Biochemistry *35*, 13222–13230.

731 Huber, W., Carey, V.J., Gentleman, R., Anders, S., Carlson, M., Carvalho, B.S., Bravo, H.C.,
732 Davis, S., Gatto, L., Girke, T., et al. (2015). Orchestrating high-throughput genomic
733 analysis with Bioconductor. Nat Methods *12*, 115–121.

734 Jang, H.-Y., Rhee, J., Carlson, J.E., and Ahn, S.-J. (2014). The Camelina aquaporin
735 CsPIP2;1 is regulated by phosphorylation at Ser273, but not at Ser277, of the C-
736 terminus and is involved in salt- and drought-stress responses. Journal of Plant
737 Physiology *171*, 1401–1412.

738 Langmead, B., and Salzberg, S.L. (2012). Fast gapped-read alignment with Bowtie 2.
739 Nat Meth *9*, 357–359.

740 Lee, S.C., Lan, W.-Z., Kim, B.-G., Li, L., Cheong, Y.H., Pandey, G.K., Lu, G., Buchanan, B.B.,
741 and Luan, S. (2007). A protein phosphorylation/dephosphorylation network
742 regulates a plant potassium channel. PNAS *104*, 15959–15964.

743 Liu, K.-H., and Tsay, Y.-F. (2003). Switching between the two action modes of the dual-
744 affinity nitrate transporter CHL1 by phosphorylation. The EMBO Journal *22*, 1005–
745 1013.

For Peer Review

Long, S., Wang, Q., and Sibley, L.D. (2016). Analysis of non-canonical calcium dependent protein kinases in Toxoplasma gondii by targeted gene deletion using CRISPR/Cas9. Infection and Immunity.

Lourido, S., and Moreno, S.N. (2015). The calcium signaling toolkit of the Apicomplexan parasites Toxoplasma gondii and Plasmodium spp. Cell Calcium *57*, 186–193.

Lourido, S., Tang, K., and Sibley, L.D. (2012). Distinct signalling pathways control Toxoplasma egress and host-cell invasion. The EMBO Journal *31*, 4524–4534.

Lourido, S., Jeschke, G.R., Turk, B.E., and Sibley, L.D. (2013). Exploiting the Unique ATP-Binding Pocket of Toxoplasma Calcium-Dependent Protein Kinase 1 To Identify Its Substrates. Acs Chemical Biology *8*, 1155–1162.

Love, M.I., Huber, W., and Anders, S. (2014). Moderated estimation of fold change and dispersion for RNA-seq data with DESeq2. Genome Biology *15*, 1–21.

Lovett, J.L., and Sibley, L.D. (2003). Intracellular calcium stores in Toxoplasma gondii govern invasion of host cells. Journal of Cell Science *116*, 3009–3016.

MacRae, J.I., Sheiner, L., Nahid, A., Tonkin, C., Striepen, B., and McConville, M.J. (2012). Mitochondrial Metabolism of Glucose and Glutamine Is Required for Intracellular Growth of Toxoplasma gondii. Cell Host & Microbe *12*, 682–692.

Marino, N.D., and Boothroyd, J.C. (2017). Toxoplasma growth in vitro is dependent on exogenous tyrosine and is independent of AAH2 even in tyrosine-limiting conditions. Exp. Parasitol.

McCoy, J.M., Whitehead, L., van Dooren, G.G., and Tonkin, C.J. (2012). TgCDPK3 regulates calcium-dependent egress of Toxoplasma gondii from host cells. PLoS Pathogens *8*, e1003066.

Mondragon, R., and Frixione, E. (1996). Ca(2+)-dependence of conoid extrusion in Toxoplasma gondii tachyzoites. The Journal of Eukaryotic Microbiology *43*, 120–127.

Moudy, R., Manning, T.J., and Beckers, C.J. (2001). The loss of cytoplasmic potassium upon host cell breakdown triggers egress of Toxoplasma gondii. Journal of Biological Chemistry *276*, 41492–41501.

Nebl, T., Prieto, J.H., Kapp, E., Smith, B.J., Williams, M.J., Yates 3rd, J.R., Cowman, A.F., and Tonkin, C.J. (2011). Quantitative in vivo Analyses Reveal Calcium-dependent Phosphorylation Sites and Identifies a Novel Component of the Toxoplasma Invasion Motor Complex. PLOS Pathogens *7*, e1002222.

Nissen-Meyer, L.S.H., Popescu, M.C., Hamdani, E.H., and Chaudhry, F.A. (2011). Protein Kinase C-Mediated Phosphorylation of a Single Serine Residue on the Rat Glial

For Peer Review

781 Glutamine Transporter SN1 Governs Its Membrane Trafficking. J. Neurosci. *31*, 6565–
782 6575.

783 Oppenheim, R.D., Creek, D.J., Macrae, J.I., Modrzynska, K.K., Pino, P., Limenitakis, J.,
784 Polonais, V., Seeber, F., Barrett, M.P., Billker, O., et al. (2014). BCKDH: the missing link
785 in apicomplexan mitochondrial metabolism is required for full virulence of
786 Toxoplasma gondii and Plasmodium berghei. PLoS Pathogens *10*, e1004263.

787 Parker, K.E.R., Fairweather, S.J., Rajendran, E., Blume, M., McConville, M.J., Broer, S.,
788 Kirk, K., and Dooren, G. van (2018). Characterization of the apicomplexan amino acid
789 transporter (ApiAT) family in Toxoplasma gondii. BioRxiv 306993.

790 Ramamoorthy, S., Shippenberg, T.S., and Jayanthi, L.D. (2010). Regulation of
791 Monoamine Transporters: Role of Transporter Phosphorylation. Pharmacology &
792 Therapeutics *129*, 220–238.

793 Rice, W.L., Zhang, Y., Chen, Y., Matsuzaki, T., Brown, D., and Lu, H.A.J. (2012).
794 Differential, Phosphorylation Dependent Trafficking of AQP2 in LLC-PK1 Cells. PLoS
795 ONE *7*, e32843.

796 Saeij, J.P.J., Boyle, J.P., Coller, S., Taylor, S., Sibley, L.D., Brooke-Powell, E.T., Ajioka, J.W.,
797 and Boothroyd, J.C. (2006). Polymorphic Secreted Kinases Are Key Virulence Factors
798 in Toxoplasmosis. Science *314*, 1780–1783.

799 Shen, B., Brown, K.M., Lee, T.D., and Sibley, L.D. (2014). Efficient gene disruption in
800 diverse strains of Toxoplasma gondii using CRISPR/CAS9. MBio *5*, e01114-14.

801 Sidik, S.M., Hortua Triana, M.A., Paul, A.S., El Bakkouri, M., Hackett, C.G., Tran, F.,
802 Westwood, N.J., Hui, R., Zuercher, W.J., Duraisingh, M.T., et al. (2016a). Using a
803 Genetically Encoded Sensor to Identify Inhibitors of Toxoplasma gondii Ca2+
804 Signalling. The Journal of Biological Chemistry.

805 Sidik, S.M., Huet, D., Ganesan, S.M., Huynh, M.-H., Wang, T., Nasamu, A.S., Thiru, P.,
806 Saeij, J.P.J., Carruthers, V.B., Niles, J.C., et al. (2016b). A Genome-Wide CRISPR Screen
807 in Toxoplasma Identifies Essential Apicomplexan Genes. Cell *166*, 1423-1435.e12.

808 Soldati, D., and Boothroyd, J.C. (1993). Transient transfection and expression in the
809 obligate intracellular parasite Toxoplasma gondii. Science *260*, 349–352.

810 Stewart, R.J., Whitehead, L., Nijagal, B., Sleebs, B.E., Lessene, G., McConville, M.J.,
811 Rogers, K.L., and Tonkin, C.J. (2016). Analysis of Ca2+ mediated signalling regulating
812 Toxoplasma infectivity reveals complex relationships between key molecules.
813 Cellular Microbiology.

814 Tamura, N., Oku, M., Ito, M., Noda, N.N., Inagaki, F., and Sakai, Y. (2013). Atg18
815 phosphoregulation controls organellar dynamics by modulating its
816 phosphoinositide-binding activity. J Cell Biol *202*, 685–698.

For Peer Review

817 Thompson, A., Schäfer, J., Kuhn, K., Kienle, S., Schwarz, J., Schmidt, G., Neumann, T., and
818 Hamon, C. (2003). Tandem Mass Tags: A Novel Quantification Strategy for
819 Comparative Analysis of Complex Protein Mixtures by MS/MS. Analytical Chemistry
820 *75*, 1895–1904.

821 Treeck, M., Sanders, J.L., Gaji, R.Y., LaFavers, K.A., Child, M.A., Arrizabalaga, G., Elias,
822 J.E., and Boothroyd, J.C. (2014). The Calcium-Dependent Protein Kinase 3 of
823 Toxoplasma Influences Basal Calcium Levels and Functions beyond Egress as
824 Revealed by Quantitative Phosphoproteome Analysis. PLOS Pathogens *10*, e1004197.

825 Wang, Z.T., Verma, S.K., Dubey, J.P., and Sibley, L.D. (2017). The aromatic amino acid
826 hydroxylase genes AAH1 and AAH2 in Toxoplasma gondii contribute to transmission
827 in the cat. PLOS Pathogens *13*, e1006272.

828 Wernimont, A.K., Artz, J.D., Finerty, P., Jr., Lin, Y.H., Amani, M., Allali-Hassani, A.,
829 Senisterra, G., Vedadi, M., Tempel, W., Mackenzie, F., et al. (2010). Structures of
830 apicomplexan calcium-dependent protein kinases reveal mechanism of activation by
831 calcium. Nature Structural & Molecular Biology *17*, 596–601.

832 Wernimont, A.K., Amani, M., Qiu, W., Pizarro, J.C., Artz, J.D., Lin, Y.H., Lew, J.,
833 Hutchinson, A., and Hui, R. (2011). Structures of parasitic CDPK domains point to a
834 common mechanism of activation. Proteins *79*, 803–820.

835 Wetzel, D.M., Chen, L.A., Ruiz, F.A., Moreno, S.N., and Sibley, L.D. (2004). Calcium-
836 mediated protein secretion potentiates motility in Toxoplasma gondii. Journal of Cell
837 Science *117*, 5739–5748.

838 Woodrow, C.J., Penny, J.I., and Krishna, S. (1999). Intraerythrocytic Plasmodium
839 falciparum expresses a high affinity facilitative hexose transporter. J. Biol. Chem. *274*,
840 7272–7277.

841

842

For Peer Review

Figure Legends

Fig 1. ApiAT5-3 localises to the plasma membrane and is phosphorylated at serine 56 upon ionophore treatment

(A) Quantification of the phosphorylation state of residues in the ApiAT5-3 N-terminus in *TgCDPK3* KOs and during ionophore-induced egress (from (Treeck et al., 2014))**.** Upper panel: The heatmap shows differential phosphorylation of S56 in *Tg*CDPK3 mutants compared to WT parasites, but not any other of the identified phosphorylation sites. Intracellular (IC) and extracellular (EC) parasites with and without 1 µM ionophore (iono). P-site = phosphorylation site. Numbers represent residue position. Black 'x' = phosphorylation site not identified. Fold changes are $\log^2$. Bottom panel: Change in relative phosphorylation of ApiAT5-3 and proteins with previously described ionophore-dependent phosphorylation sites, measured after addition of 8 µM ionophore over 60 s. Numbers after the identifier represent the phosphorylation site quantified. **(B)** ApiAT5-3 was detected by Western blot analysis of ApiAT5-3::HA cell lysate using an anti-HA antibody. Loading control anti-Toxo. **(C)** IFA of ApiAT5-3::HA expressing parasites shows that ApiAT5-3 localises to the periphery of the intracellular tachyzoite. Red = HA, Green = SAG1, Blue = DAPI. Scale bar 5 µm.

Fig 2. ApiAT5-3 is essential for parasite proliferation

(A) Generation of the ApiAT5-3_loxP line using CRIPSPR/Cas9 to increase site-directed integration. Protospacer adjacent motif (PAM) indicated by black arrows. Primer pairs represented by coloured triangles. **(B)** Left panel: PCR analysis shows

For Peer Review

correct integration of the ApiAT5-3_loxP construct at both the 3' and 5' ends and a loss of WT *apiAT5-3* at the endogenous locus. White * = non-specific bands. Right panel: Addition of RAP leads to correct recombination of the loxP sites. **(C)** Fluorescent microscopy of ApiAT5-3_loxP parasites 24 hrs after addition of DMSO or RAP. Scale bar 5 µm **(D)** Plaque assay showing loss of plaquing capacity of ApiAT5-3_loxP parasites upon RAP-treatment. **(E)** Parasite per vacuole number shown as mean %, n = 3 **(F)** Stills from live video microscopy at 36, 42 and 45 hrs into 3rd lytic cycle post RAP-treatment. Red = RH Tom, dashed white line = intact WT ApiAT5-3_loxP vacuoles, green = *apiAT5-3* KO. Scale bar 20 µm. **(G)** IIE assay showing no significant difference between DMSO and RAP-treated ApiAT5-3_loxP (at 30 hrs into lytic cycle 2 post DMSO/RAP-treatment). Statistical analysis using multiple comparison 2-way ANOVA, n = 2.

Fig 3. Δ*apiAT5-3* parasites display a transcriptional response related to amino acid starvation

(A) Extracted reads for recodonised *apiAT5-3* from RNA sequence data show a significant reduction of *apiAT5-3* transcripts in RAP-treated ApiAT5-3_loxP lines 60 hrs post RAP-treatment compared to RAP-treated ApiAT5-3_loxP^{dDiCre} parasites. **(B)** Heatmap of genes that change significantly (adjusted p <0.05) in transcript read number between WT and Δ*apiAT5-3* 60 hrs post addition of RAP. **(C)** Gene ontology term enrichment shows that genes involved in translation processes are significantly enriched among the differentially expressed genes 60 hrs post RAP-treatment.

For Peer Review

889 **Fig 4. Δ*apiAT5-3*$^{\text{ApiAT5-3\_S56A}}$ demonstrates a fitness defect**

890 **(A)** Generation of the ApiAT5-3$^{\text{ApiAT5-3/_S56A/_S56D}}$ complementation lines. PAM
891 indicated by black arrow. Primer pairs represented by coloured triangles. **(B)** PCR
892 analysis shows correct integration of the ApiAT5-3_loxP construct at both the 3' and
893 5' ends and a loss of *uprt*. White * = non-specific band **(C)** IFA of ApiAT5-3$^{\text{ApiAT5-}}$
894 $^{\text{3/\_S56A/\_S56D::HA}}$ expressing parasites shows that ApiAT5-3 is correctly trafficked to the
895 periphery of the intracellular tachyzoite in both the presence (DMSO) and absence
896 (RAP) of the endogenous *apiAT5-3*. Red = HA. Green = YFP, indicating correct excision
897 of the endogenous *apiAT5-3.* Scale bar 10 μm. **(D)** Geometric mean of red fluorescence
898 calculated by flow cytometric analysis of complemented parasites, probed with red
899 fluorescent anti-HA antibody. Statistical analysis carried out using multiple
900 comparison, 2-way ANOVA, ns = not significant. All complemented lines differ
901 significantly in mean fluorescence from ApiAT5-3_loxP ($p<0.0001$), n = 3. **(E)** Growth
902 competition assay by flow cytometry shows that Δ*apiAT5-3*$^{\text{ApiAT5-3\_S56A}}$ parasite
903 growth is reduced relative to the non-excised ApiAT5-3$^{\text{ApiAT5-3_S56A}}$ line. Statistical
904 analysis using multiple comparison, 2-way ANOVA of mean ratio to day 0 normalised
905 to 1. ***$p <0.001$, n = 3.
906

907 **Fig 5. Functional analysis of the ApiAT5-3 transporter**

908 **(A)** *X. laevis* oocytes expressing ApiAT5-3 demonstrate a significant increase in ^{14}C-
909 L-tyrosine uptake. 10 oocytes per experiment. Analysis carried out using a two-tailed,
910 paired, Student's t-test. ***$p <0.001$ Box plots show mean, 1st and 3rd quartile and SD,
911 n = 5. **(B)** Extracellular, RAP-treated, ApiAT5-3_loxP tachyzoites, labelled with ^{13}C-L-

For Peer Review

tyrosine or ^{13}C-L-isoleucine, display a marked decrease in tyrosine but not isoleucine import, relative to WT, n = 2. **(C)** Plaque assay shows no rescue of growth of RAP-treated ApiAT5-3_loxP on addition of excess (2 mM) L-tyrosine.

Supporting information

Graphical abstract

ApiAT5-3, a 12-transmembrane domain protein that localises to the periphery of the parasite, is responsible for the import of tyrosine, and is essential for parasite survival. *Tg*CDPK3 mediates phosphorylation (blue star) at the S56 residue and may be involved in the regulation of tyrosine uptake from the host.

S1 Fig. ApiAT5-3_loxP parasites that survive RAP-treatment retain the *apiAT5-3* gene.

(**A**) PCR analysis using primers spanning the floxed *apiAT5-3* gene show that the small proportion of non-excised parasites present after RAP-treatment outgrow the excised Δ*apiAT5-3* parasites within 2 weeks. (**B**) PCR analysis using primers spanning the floxed *apiAT5-3* gene of ApiAT5-3_loxp (DiCre (+)) and ApiAT5-3_loxp^{dDiCre} (DiCre (-)). (**C**) Plaque size of RAP- compared to DMSO-treated ApiAT5-3_loxP parasites after 9 days of growth. White dotted line = plaque outline. Green = YFP (*apiAT5-3* KO parasites). Scale bar 200 μm.

S2 Fig. Verification of ApiAP5-3 complementation lines.

(A) Addition of RAP to the complemented parasite lines leads to correct recombination of the loxP sites and deletion of the endogenous *apiAT5-3* gene. **(B)**

For Peer Review

Plaque assay showing restoration of plaquing efficiency upon RAP-treatment of the ApiAT5-3_loxP line complemented with the WT or phosphomutant versions of the gene.

S3 Fig. Analysis of ApiAP5-3 transport function.

(A) *X. laevis* oocytes expressing *apiAT5-3* demonstrate an increase in ^{14}C-L-phenylalanine uptake but no significant ^{14}C-L-valine uptake. 10 oocytes per experiment. Analysis carried out using a two-tailed, paired, Student's t-test. *p <0.05, ns = non-significant. n = 2. **(B)** Relative abundance of amino acids in RAP-treated ApiAT5-3_loxP (KO) relative to Δ*apiATP5-3*$^{\text{ApiAT5-3}}$ (WT), shows that tyrosine is the most significantly reduced upon loss of ApiAT5-3. **(C)** Tyrosine abundance in normal DMEM compared to DMEM supplemented with 2 mM tyrosine. (**D**) Plaque formation of *apiAT5*-3_loxP RAP-treated parasites is not restored on the addition of 2 mM exogenous phenylalanine. (**E**) Extracellular Δ*apiAT5-3*$^{\text{apiAT5-3\_S56A}}$ and Δ*apiAT5-3*$^{\text{apiAT5-3\_S56D}}$ tachyzoites labelled with ^{13}C-L-tyrosine do not display a marked difference in tyrosine import, n = 3. **(F)** *X. laevis* oocytes expressing *apiAT5-3_S56A* demonstrate a modest but insignificant reduction in ^{14}C-L-tyrosine uptake relative to *apiAT5-3* and *apiAT5-3_S56D*. 10 oocytes per experiment ****p <0.0001, ns = non-significant. Analysis carried out using multiple comparison, one-way ANOVA. Box plots show mean, 1st and 3rd quartile and SD, n = 5.

For Peer Review

S1 Movie. Live video microscopy of Δ*apiAT5-3* parasites

Live video microscopy of ApiAT5-3_loxP parasites 29 hrs into the 3rd lytic cycle post DMSO- **(A)** or RAP- **(B)** treatment. Red = WT RH Tom, colourless parasites = non-excised ApiAT5-3_loxP, green parasites = YFP expressing *apiAT5-3* KO. Scale bar 20 µm.

S1 Table. Phosphoproteome time course data for selected peptides after ionophore treatment.

Log^2 fold changes (red) on selected phosphorylation sites after 0 (DMSO), 15, 30 and 60 seconds post ionophore treatment.

S2 Table. RNA sequencing analysis of *apiAT5-3* conditional KO

A list of all genes displaying log^2 fold change in the RAP-treated Δ*apiAT5-3*$^{ApiAT5-3}$ compared to ApiAT5-3_loxP parasites, 4 and 60 hrs after RAP-treatment.

S3 Table. Primers and synthetic DNA sequences used throughout this study.

S4 Table. *Toxoplasma gondii* strains generated throughout this study.

For Peer Review

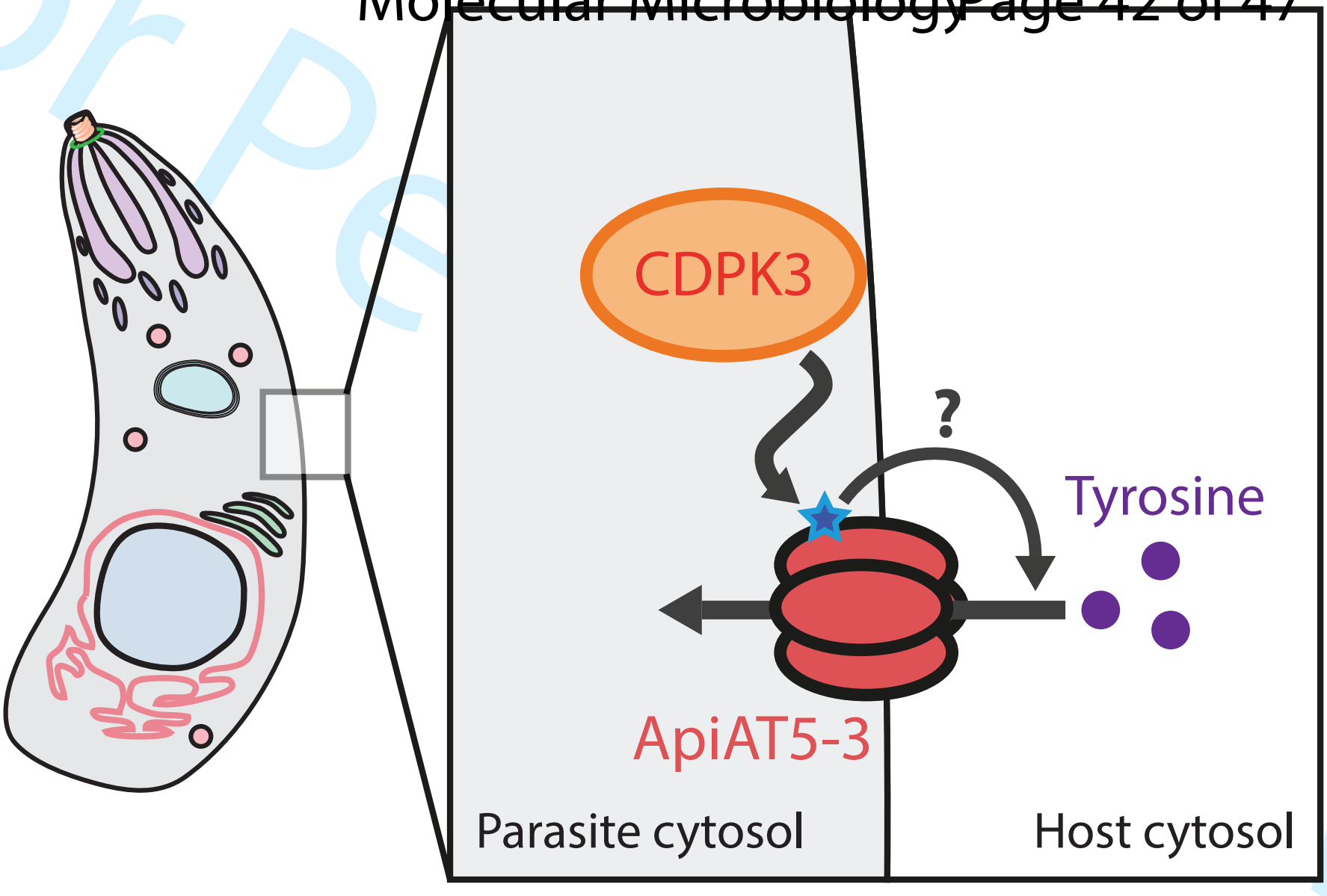
CDPK3
?
Tyrosine
ApiAT5-3
Parasite cytosol
Host cytosol

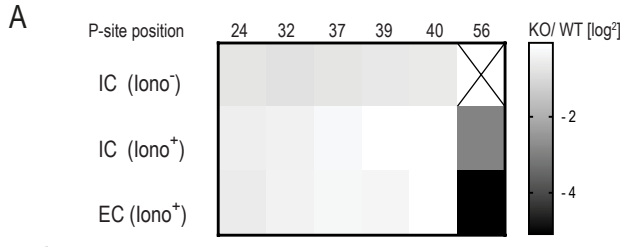
A
P-site position
24
32
37
39
40
56
KO/ WT [log2]
IC (Iono-)
IC (Iono+)
EC (Iono+)
-2
-4

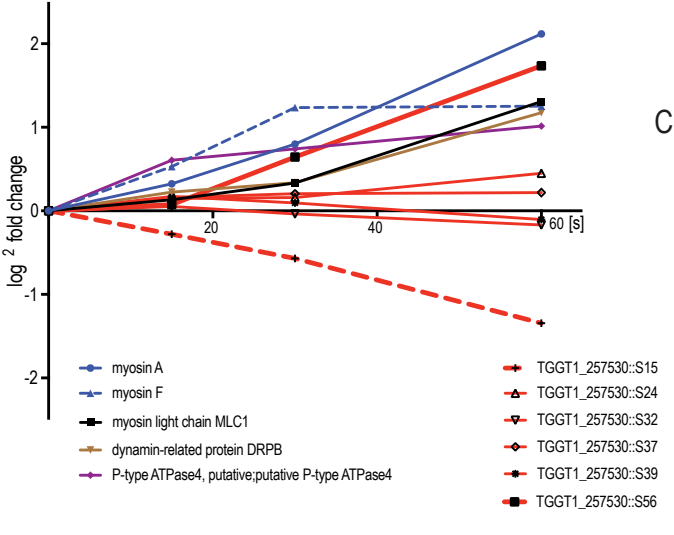
log 2 fold change
2
1
0
-1
-2
20
40
60 [s]
myosin A
myosin F
myosin light chain MLC1
dynamin-related protein DRPB
P-type ATPase4, putative;putative P-type ATPase4
TGGT1_257530::S15
TGGT1_257530::S24
TGGT1_257530::S32
TGGT1_257530::S37
TGGT1_257530::S39
TGGT1_257530::S56

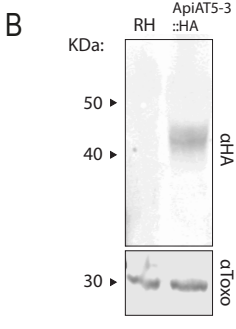
B
RH
ApiAT5-3 ::HA
KDa:
50
40
30
αHA
αToxo

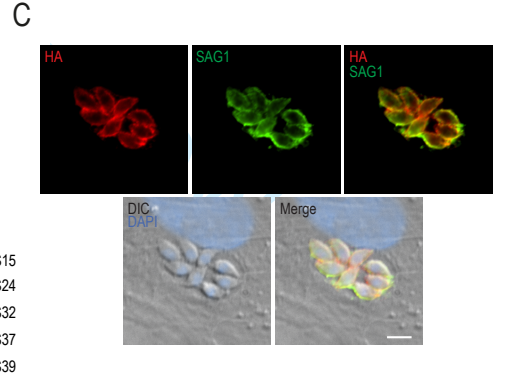
C
HA
SAG1
HA
SAG1
DIC
DAPI
Merge

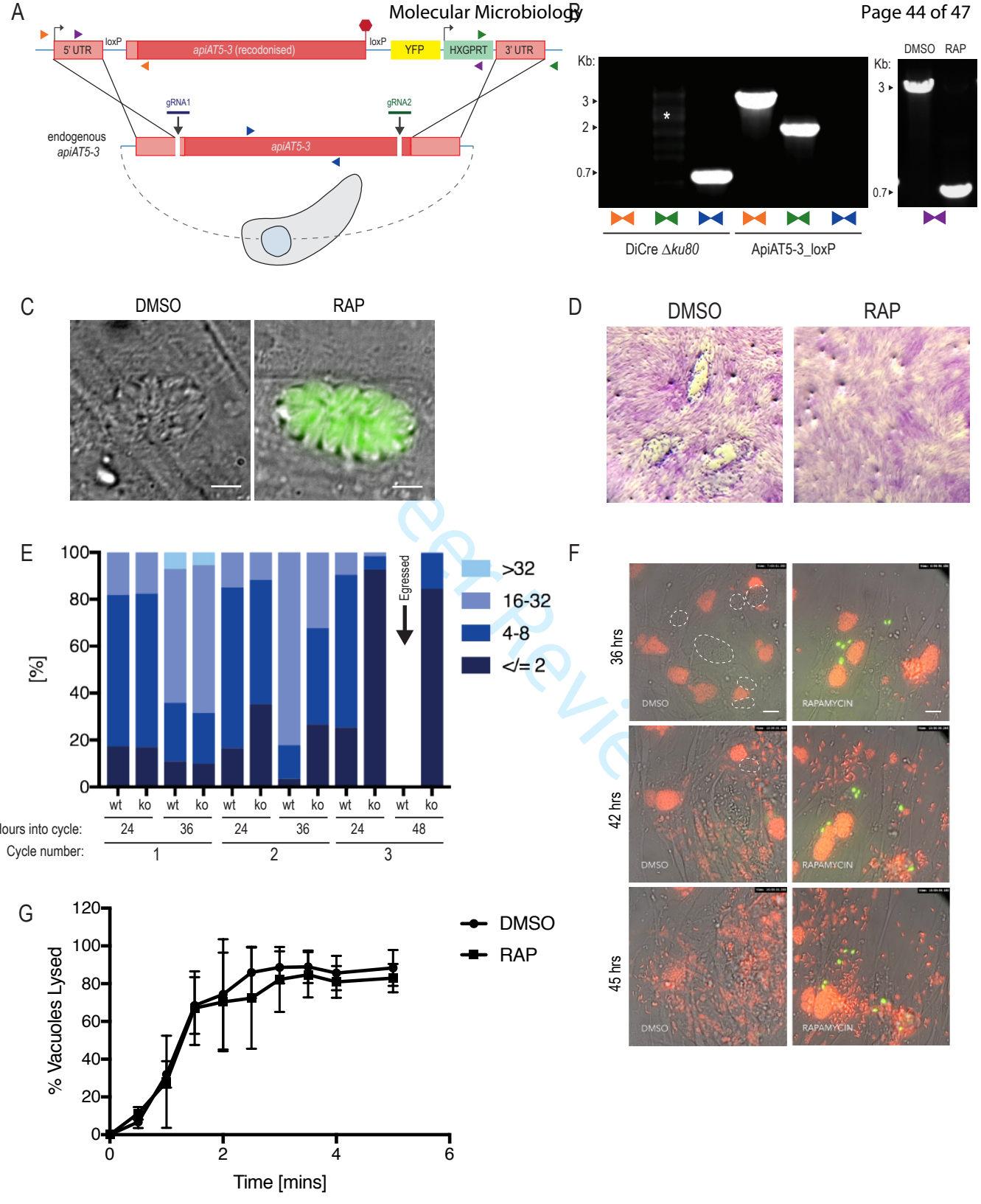
A
5' UTR
loxP
apiAT5-3 (recodonised)
loxP
YFP
HXGPRT
3' UTR
gRNA1
gRNA2
endogenous apiAT5-3
apiAT5-3
B
Kb:
3
2
0.7
*
DMSO
RAP
DiCre Δku80
ApiAT5-3_loxP
C
DMSO
RAP
D
DMSO
RAP
E
[%]
Egressed
>32
16-32
4-8
</= 2
wt ko wt ko wt ko wt ko wt ko wt ko
Hours into cycle: 24 36 24 36 24 48
Cycle number: 1 2 3
F
36 hrs
42 hrs
45 hrs
DMSO
RAPAMYCIN
G
% Vacuoles Lysed
Time [mins]
DMSO
RAP

For Review

A

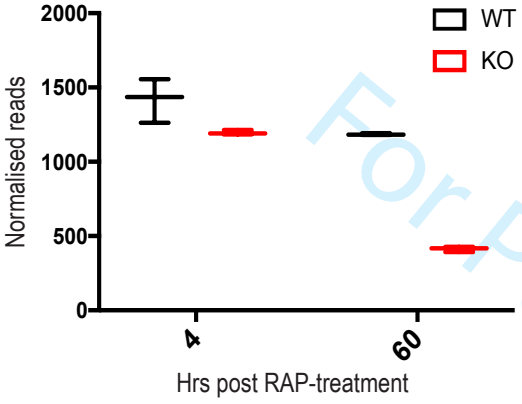

B

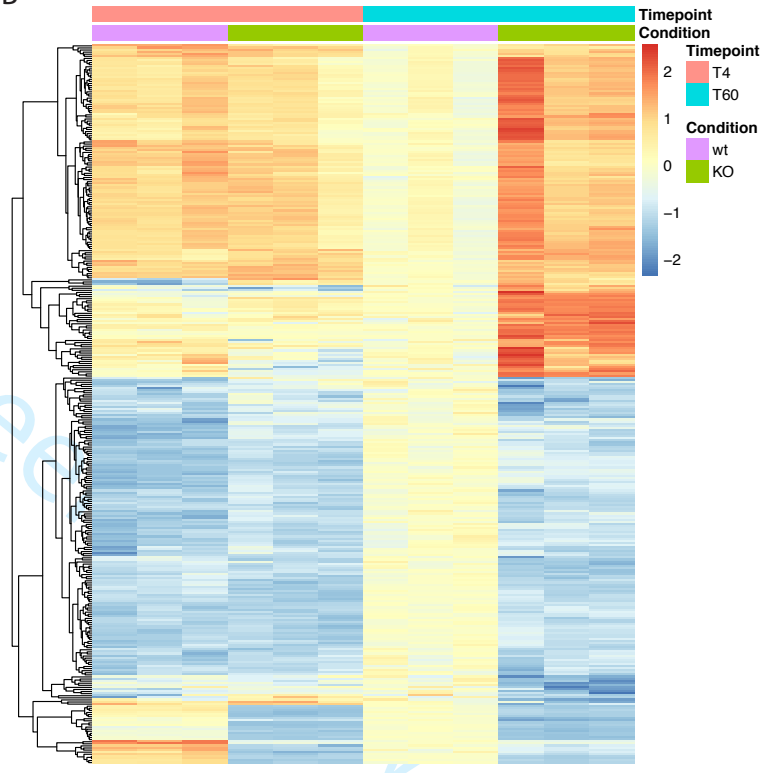

C

Biological process	Enrichment	Odds ratio	P-value	Benjamini	Bonferroni
translation	5.41	10.79	5.75E-38	1.38E-36	1.38E-36
biosynthetic process	2.65	4.06	2.28E-19	2.73E-18	5.46E-18
cellular nitrogen compound metabolic process	2.15	3.09	3.48E-14	2.78E-13	8.35E-13
biological process	1.26	1.93	1.77E-06	1.06E-05	4.25E-05
cellular protein modification process	1.42	1.52	4.60E-02	2.21E-01	1.00E+00

For Peer Review

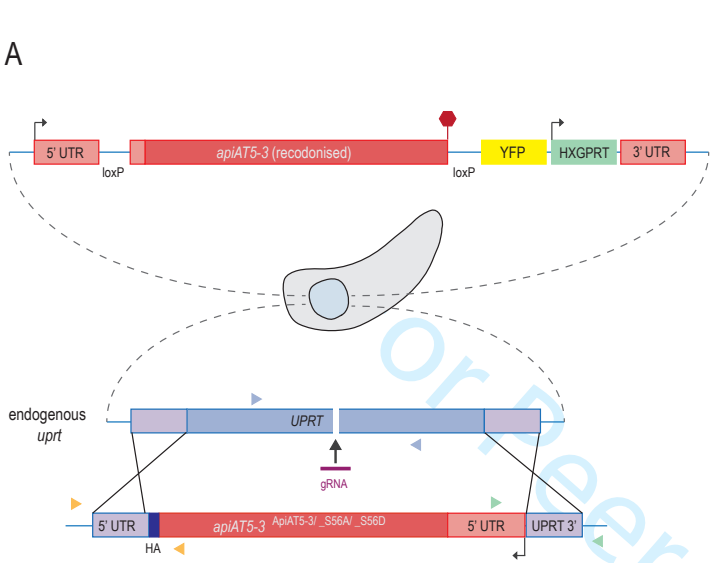

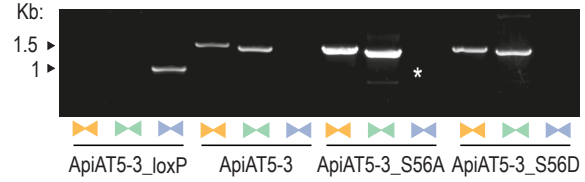

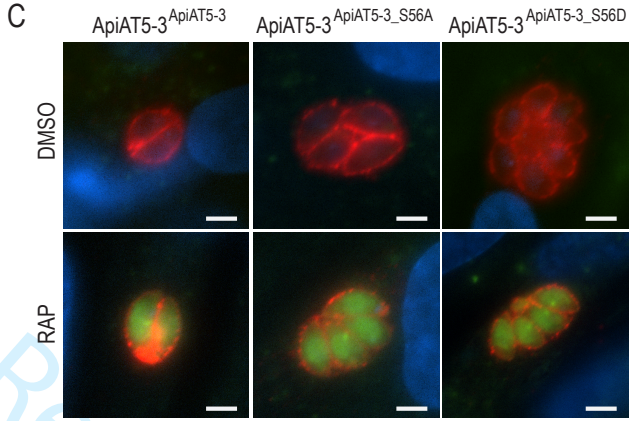

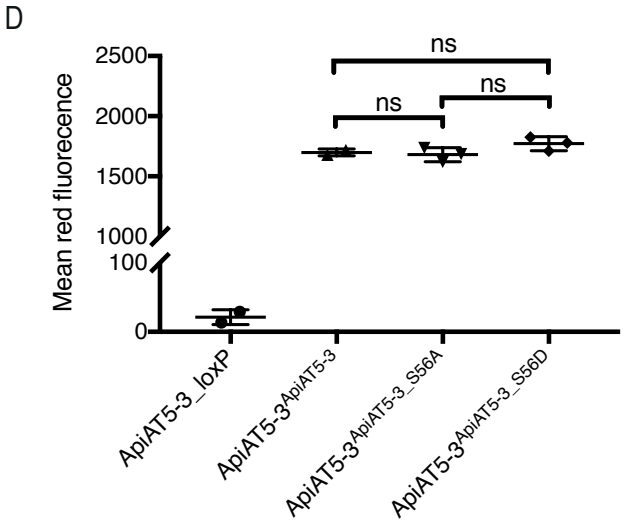

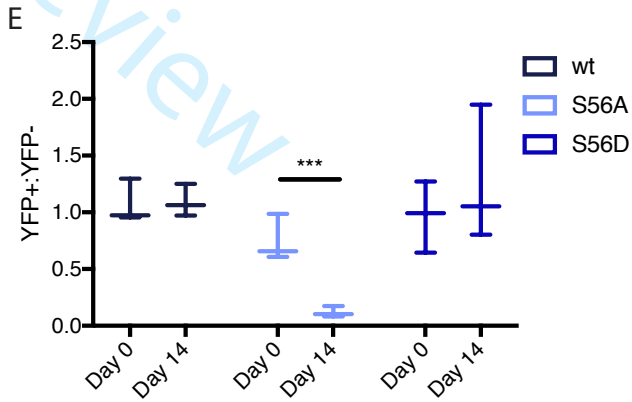

For Peer Review

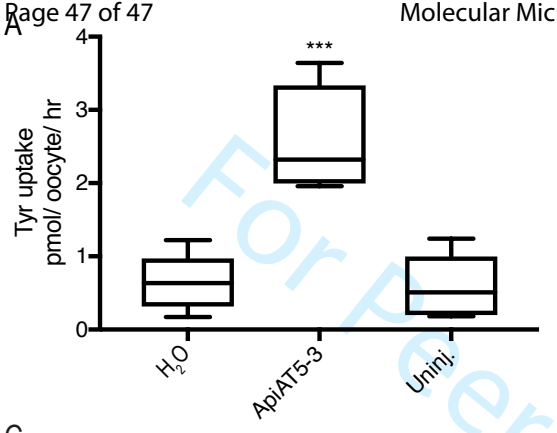

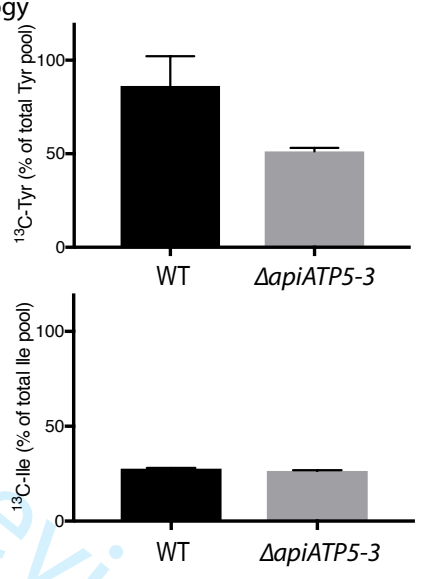

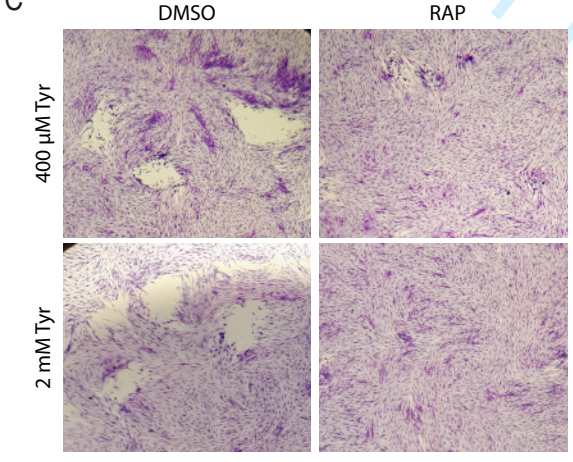

For Peer Review